

Chapter 5

Temperature Dependence of the Interfacial Reaction between Titanium and Zirconia Annealed between 1100° and 1550°C

5.1 Introduction

The interface reactions between titanium and zirconia have been studied in the past several decades,¹⁻³ and it is generally accepted that oxygen was readily dissolved into the titanium to form α -Ti(O), resulting in the blackening of oxygen deficient zirconia (ZrO_{2-x}). The various reaction layers in the interface between titanium and zirconia were found,⁴⁻⁵ however, they were not fully explored because of the limitations of the analytical instruments. Meanwhile, some researchers⁶⁻⁷ indicated that the titanium additive could improve the mechanical properties of zirconia including strength and thermal shock resistance.

Recently, Lin and his coworkers⁸⁻¹¹ have thoroughly investigated the diffusional reaction between titanium and zirconia. Using TEM/EDS analyses, they indicated that an ordered titanium suboxide (Ti_3O) and the orthorhombic lamellae Ti_2ZrO were formed in the solid solution of α -Ti(O) between zirconia and titanium melt during cooling from 1700°C. In addition to the lamellar Ti_2ZrO and α -Ti(O), the orthorhombic β' -Ti(Zr, O) and an spherical ordered Ti_2ZrO phase were also found in the metal side of the Ti/ ZrO_2 diffusion couple after annealing at 1550°C.⁹ The orientation relations between the α -Ti (Zr, O) and lamellae Ti_2ZrO were determined to be $[0001]_{\alpha-Ti} // [110]_{Ti_2ZrO}$ and $(10\bar{1}0)_{\alpha-Ti} // (1\bar{1}0)_{Ti_2ZrO}$; meanwhile those between the α -Ti(O) and the spherical ordered Ti_2ZrO were $[0001]_{\alpha-Ti} //$

$[0001]_{\text{Ti}_2\text{ZrO}}$ and $(10\bar{1}0)_{\alpha\text{-Ti}} // (10\bar{1}0)_{\text{Ti}_2\text{ZrO}}$. Furthermore, the acicular $\alpha\text{-Ti(O)}$ was precipitated in the $\beta'\text{-Ti(O, Zr)}$ matrix with two various sets of orientation relations in the metal side.¹⁰ One set of the orientation relations was determined to be $[2\bar{1}\bar{1}0]_{\alpha\text{-Ti}} // [001]_{\beta'\text{-Ti}}$ and $(0001)_{\alpha\text{-Ti}} // (100)_{\beta'\text{-Ti}}$ and the other was $[2\bar{1}\bar{1}0]_{\alpha\text{-Ti}} // [021]_{\beta'\text{-Ti}}$ and $(0001)_{\alpha\text{-Ti}} // (1\bar{1}2)_{\beta'\text{-Ti}}$.¹⁰ In the zirconia side far away from the interface of Ti/ZrO₂, Lin and Lin¹¹ also observed twinned $t'\text{-ZrO}_{2-x}$, lenticular $t\text{-ZrO}_{2-x}$, and/or ordered $c\text{-ZrO}_{2-x}$ as well as the intergranular $\alpha\text{-Zr}$ after annealing at 1550°C.

Even though extensive studies were carried out on the interface reaction between the titanium and zirconia, the temperature effect on the microstructure evolution has not been elucidated to date. It was noticeable that the temperature effect was of a great influence on the microstructural development in the interface between titanium and zirconia. In order to shed light on the temperature effect on the microstructural evolution of the various distinct reaction layers between titanium and zirconia, the Ti/ZrO₂ diffusion couples were isothermally annealed in argon at 1100°, 1300°, 1400°, and 1550°C, respectively, for 6 hours in the present study. The microstructures were characterized using analytical scanning electron microscopy (SEM) and transmission electron microscopy (TEM), both attached an energy dispersive spectrometer (EDS). The microstructures developed at various temperatures were then compared and explained by the diffusion paths in the Ti-Zr-O ternary phase diagram.

5.2 Experimental Procedures

5.2.1 Sample Preparation

Bulk ZrO₂ specimens were prepared from the powder of 3 mol% Y₂O₃ partially stabilized zirconia by the hot-press (Model HP50-MTG-7010,

Thermal Technology Inc., Santa Rosa, CA). The nominal composition of the zirconia was supplied by the vendor (Toyo Soda Mfg. Co., Tokyo, Japan) as follows: > 94 wt% ZrO₂ + HfO₂ (accounting for approximately 2~3% of this total), 5.4 wt% Y₂O₃, < 0.001 wt% Fe₂O₃, < 0.01 wt% SiO₂, < 0.005 wt% Na₂O, < 0.005 wt% TiO₂, < 0.02 wt% Cl, < 0.005 wt% SO₄²⁻. The bulk ZrO₂ and available titanium billets (with a nominal composition of 99.31 wt% Ti, 0.25 wt% O, 0.01 wt% H, 0.03 wt% N, 0.10 wt% C, 0.30 wt% Fe; Kobe Steel, Ltd., Tokyo, Japan) were cut and machined to the dimension of 14 mm x 14 mm x 5 mm. One Ti billet was inserted in between two ZrO₂ specimens to form a sandwiched sample. The sandwiched samples were slightly pressed and annealed at 1100°, 1300°, 1400°, and 1550°C, respectively, for 6 hour at an atmospheric argon. The hot-pressing procedures of both bulk ZrO₂ and the sandwiched samples have been described in detail elsewhere.⁹

5.2.2 Sample Observation

5.2.2.1 SEM/EDS analyses

An SEM (Model JSM-6330F, JEOL Ltd., Tokyo, Japan) equipped with an energy-dispersive spectrometer (EDS, Mode ISIS300, Oxford Instrument Inc., London, UK) was used for the microstructure observation in the interface between titanium and zirconia. Both backscattering electron image (BEI) and secondary electron image (SEI) were acquired. Cross-sectional specimens were cut into about 3 mm x 2 mm x 1 mm, and then ground and polished by diamond paste down to 1 μm. The specimens for the SEI observation were etched by the Kroll reagent (10 ml HF + 30 ml HNO₃ + 60 ml H₂O) for 15 seconds. In order to avoid electric charging under the electron beam, specimens were coated with a thin layer of platinum.

5.2.2.2 TEM/EDS analyses

A TEM (Model JEM 2000Fx, JEOL Ltd., Tokyo, Japan) equipped with an energy-dispersive spectrometer (EDS, Mode ISIS300, Oxford Instrument Inc., London, UK) was also employed for characterizing the microstructure at the interface between titanium and zirconia. Cross-sectional TEM specimens perpendicular to the interface of titanium and zirconia were cut, ground, and polished by standard procedures mentioned previously.⁹ The TEM specimens were dimpled and ion milled by a precision ion miller (Model 691, Gatan Inc., Pleasanton, CA). The quantitative composition analyses were carried out based on the principle of the Cliff-Lorimer standardless technique¹² by the EDS attached to the TEM. In order to avoid electric charging under the electron beam, all the TEM specimens were coated with a thin film of carbon.

5.3 Results and Discussion

5.3.1 Distinct microstructures at various temperatures

Figure 5.1 displays the backscattered electron images (BEI) of the cross-section normal to the Ti/ZrO₂ interface after annealing at 1100°, 1300°, 1400°, and 1550°C for 6 hours, respectively. Titanium was in the left-hand side, while zirconia was in the other side. The vertical arrows in the upper side indicate the original interface of Ti and ZrO₂. The original interface was deliberately located by the results of characteristic K_{α} x-ray maps of yttrium (not shown), which was relatively immobile compared with elements Zr, O, and Ti. A large amount of the pores existed in the ceramic side after annealing at 1550°C. The formation of these pores was attributed to the Kirkendall effect, because zirconium and oxygen diffused to the titanium side much faster than titanium did toward the zirconia side in the opposite direction.

It was obvious that the microstructure the Ti/ZrO₂ interface strongly depended upon the annealing temperature. A gray thin layer (designed as the reaction layer “I”) was formed in the interface reaction between Ti and ZrO₂ at all temperatures above 1400°C as shown in Fig. 5.1(c) and (d). The reaction layers “I” in Fig. 5.1(a) and (b) were invisible because of the limited resolution, however, they could be observed using SEM or TEM at a higher magnification [Fig. 5.2(a) and Fig. 5.3(a)]. To the left of the reaction layer “I” is the α -Ti with oxygen in solid solution, designated as α -Ti(O) in this study.

The lamellar α -Ti(Zr, O) and Ti₂ZrO along with β' -Ti(Zr, O) (designed as the reaction layer “II”), as indicated previously,⁹ were observed only in the Ti/ZrO₂ interface after annealing at 1550°C/6 h (Fig. 5.1(d) and Fig. 5.4). The β -Ti phase, which dissolved a large amount of Zr and O at high temperatures, was transformed to the orthorhombic β' -Ti(Zr, O) solid solution during cooling, while the Ti₂ZrO lamellae were precipitated from α -Ti (Zr, O) during cooling.⁹

The acicular α -Ti(Zr, O) and β' -Ti(Zr, O) co-existed in the region designed as the reaction layer “III” after annealing at 1400°C or 1550°C as shown in Fig. 5.1(c) and (d). At a higher magnification, it was seen that the amount of acicular α -Ti(Zr, O) gradually decreased towards the original interface.¹⁰

The region abutting the original interface dissolved a higher concentration of Zr in titanium. No acicular α -Ti(Zr, O) was thus observed in this region since the zirconium was an effective stabilizer of β -Ti. Figures 5.1(b), (c) and (d) show that a continuous β' -Ti(Zr, O) layer (designed as the reaction layer “IV”) was formed in the metal side abutting the original interface after annealing at temperatures ranging from 1300°C to 1550°C.

Figure 5.1 also demonstrates very distinct microstructures after annealing at various temperatures in the ceramic side. At 1100°C, the anneal temperature was so low that no apparent interfacial reaction was noticeable. At higher temperatures above 1300°C, zirconia was gradually dissolved in titanium so that residual fine spherical c -ZrO₂ existed in β' -Ti(Zr, O). The spherical zirconia contained a significant amount of Y₂O₃, resulting in the stabilization of c -ZrO_{2-x} (designated as the reaction layer “V”) as shown particularly in Fig. 5.1(c) and (d). It is believed that, at high temperatures such as 1400°C or 1550°C, the reaction enhanced dissolution of ZrO₂ into Ti is an important mechanism taking place at the reaction layer “V.”

On being taken in contact with Ti, zirconia would lose oxygen and became oxygen deficient at higher temperatures, that is, zirconia was reduced. As mentioned previously,¹¹ at high temperatures, the extremely vehement oxidation-reduction reaction resulted in the formation of metastable oxygen deficient zirconia (ZrO_{2-x}). Then α -Zr would be excluded from this metastable ZrO_{2-x} to the grain boundaries of zirconia during the subsequent cooling. In the layer “VI” as shown in Fig. 5.1(b)-(d), the intergranular α -Zr coexisted with tetragonal and/or cubic zirconia mentioned in the previous studies.¹¹ At 1300°C, the negligible grain growth of zirconia resulted in the finely dense distribution of α -Zr as shown in Fig. 5.1(b). For the sample after annealing at 1400°C, zirconia were delineated by the continuously distributed intergranular α -Zr [Fig. 5.1(c)], indicating a significant grain growth. In addition to the apparent grain growth of zirconia, the intergranular α -Zr was coarsened and became isolated, as shown in Fig 5.1(d), after annealing at 1550°C.

5.3.2. Variation in the reaction layer “I”

When Ti was brought in contact with ZrO₂ at high temperatures, oxygen and

zirconium from ZrO_2 were dissolved into Ti, resulting in α -Ti with oxygen and zirconium in solid solution. Compared with a limited diffusion range of zirconium (up to the reaction layer “I”), oxygen showed a relatively long diffusion range (beyond the reaction layer “I”). Rather than forming a distinct layer with a specific thickness, the oxygen concentration of α -Ti(O) decayed gradually across a wide region.

The nearest neighboring layer of α -Ti(O) was the reaction layer “I,” consisting of the lamellar α -Ti(Zr, O) and Ti_2ZrO . On annealing, the dissolution of a large amount of zirconium and oxygen into titanium gave rise to the body-centered cubic β -Ti (Zr, O). During the subsequent cooling, the β -Ti(Zr, O) was transformed to the metastably supersaturated disordered α -Ti(Zr, O) solid solution where the Ti_2ZrO phase was subsequently precipitated.

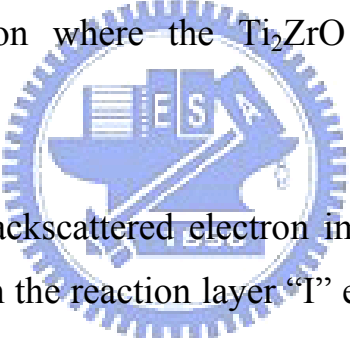


Figure 5.2 displays the backscattered electron image (BEI) of the lamellar α -Ti (Zr, O) and Ti_2ZrO in the reaction layer “I” etched by Kroll reagent (10 ml HF + 30 ml HNO_3 + 60 ml H_2O) after annealing at 1300°, 1400°, and 1550°C, respectively. The thickness of the reaction layer “I” increased with temperature. Figure 5.2 shows clearly, at higher magnifications, the very different microstructures developed at various anneal temperatures. For example, the sequence of the reaction layers I + IV + ... [Fig. 5.2(a)] was formed after annealing at 1300°C, while the sequence of the reaction layers I + III + ... [Fig. 5.2(b)] and the sequence of the reaction layers I + II + ... [Fig. 5.2(c)] are formed, respectively, after annealing at 1400°C and at 1550°C.

For the benefit of the higher resolution of TEM, a very thin reaction layer “I” was found in the Ti/ ZrO_2 interface after annealing at 1100°C for 6 h. Figure 5.3(a) displays the TEM micrograph of the cross-section between Ti

and ZrO_2 after annealing at 1100°C for 6 h. The arrow indicated the original interface with titanium and zirconia being in the upper and lower sides, respectively. The lamellar phases were identified to be orthorhombic Ti_2ZrO and hexagonal disordered $\alpha\text{-Ti}(\text{Zr}, \text{O})$, respectively, from the superimposed selected area diffraction patterns (SADPs) shown in Fig 5.3(b). The orientation relations were determined to be $[0001]_{\alpha\text{-Ti}} // [110]_{\text{Ti}_2\text{ZrO}}$ and $(10\bar{1}0)_{\alpha\text{-Ti}} // (1\bar{1}0)_{\text{Ti}_2\text{ZrO}}$. Figure 5.3(c) shows the EDS spectrum of the lamellar Ti_2ZrO , consisting of 56.10 at.% Ti, 22.89 at.% Zr, and 21.01 at.% O.

5.3.3 Formation of the reaction layer “II” at 1550°C

As shown in Fig. 5.1(d) and Fig. 5.2(c), The reaction layer “II” consists of the interlaced Ti_2ZrO and $\alpha\text{-Ti}$ as well as $\beta'\text{-Ti}$.

The superimposed SADPs of lamellar $\alpha\text{-Ti}(\text{Zr}, \text{O})$ and Ti_2ZrO were shown in the upper right corner of Fig. 5.4 and the orientation relationship was determined to be $[0001]_{\alpha\text{-Ti}} // [110]_{\text{Ti}_2\text{ZrO}}$ and $(10\bar{1}0)_{\alpha\text{-Ti}} // (1\bar{1}0)_{\text{Ti}_2\text{ZrO}}$, which was consistent with the previous results presented by Lin and Lin.^{8,9}

The formation mechanism of the reaction layer “II” can be described by the aid of the Ti-ZrO_2 phase diagram.¹³ It is known from the Ti-ZrO_2 phase diagram that hexagonal $\alpha\text{-Ti}$ and body-centered cubic $\beta\text{-Ti}$ coexist in Cp-Ti at 1550°C . At such a high temperature, the primary $\alpha\text{-Ti}$ dissolved zirconium and oxygen, forming the metastable $\alpha\text{-Ti}(\text{Zr}, \text{O})$. During the subsequent cooling, the precipitation of the lamellae Ti_2ZrO in the metastable $\alpha\text{-Ti}(\text{Zr}, \text{O})$ occurred. Meanwhile, the $\beta\text{-Ti}$, with a large amount of Zr and O in solid solution, was transformed to orthorhombic $\beta'\text{-Ti}(\text{Zr}, \text{O})$ during cooling, since Zr is an effective stabilizer of the $\beta\text{-Ti}$ phase.

5.3.4 Variation of the reaction layer “III”

Unlike annealing at 1550°C, the acicular α -Ti(Zr, O) and β' -Ti(Zr, O), instead of β' -Ti, α -Ti, and Ti_2ZrO [the reaction layer “II” in Fig. 5.1(d) and Fig. 5.3(c)], coexisted to form the reaction layer “III” [Fig. 5.1(c) and Fig. 5.2(b)] in the Ti/ZrO₂ interface after annealing at 1400°/6 h. Below the annealing temperatures as 1300°C, the reaction layer “III” was not found due to a limited reaction between Ti and ZrO₂. The reaction layer “III” appeared as a relatively minor layer at 1550°C along with the reaction layer “II,” as shown in Fig. 5.1(c).

From the inset SADPs in the upper right corner of Fig. 5.5(a), the orientation relationship of α -Ti and β' -Ti in the reaction layer “III” was determined to be $[2\bar{1}\bar{1}0]_{\alpha\text{-Ti}} // [001]_{\beta'\text{-Ti}}$ and $(0001)_{\alpha\text{-Ti}} // (100)_{\beta'\text{-Ti}}$. Similarly, the other orientation relationship of the acicular α -Ti and the β' -Ti was identified from the inset SADPs of Fig. 5.5(b) as follows: $[2\bar{1}\bar{1}0]_{\alpha\text{-Ti}} // [021]_{\beta'\text{-Ti}}$ and $(0001)_{\alpha\text{-Ti}} // (1\bar{1}2)_{\beta'\text{-Ti}}$. These two different orientation relations between the acicular α -Ti(Zr, O) and β' -Ti(Zr, O) in the reaction layer “III” were consistent with Lin and Lin report.¹⁰ They indicated that the acicular α -Ti was precipitated from β' -Ti matrix by means of the ledge mechanism.

5.3.5 Variation in the reaction layer “V”

The reaction layer “V” along with the reaction layer “VI” is located in the original ceramic side. This layer existed in the interface between titanium and zirconia after annealing above 1300°C.

Figure 5.6(a) shows the bright field image (BFI) of the reaction layer “V” after annealing at 1400°C for 6 h. The reaction layer “V,” in the outermost region of the original zirconia, consists of β' -Ti(Zr, O) and $c\text{-ZrO}_{2-x}$. It is believed that titanium diffused into zirconia along grain boundaries, where

the zirconia was gradually dissolved into titanium and became rounded in shape, resulting in β -Ti with oxygen and zirconium in solid solution. Since the solubility of yttrium, the stabilizer of ZrO_2 in the present study, in titanium was quite limited, yttrium was retained in the residual cubic zirconia. It is consistent with the results reported by Zhu *et al.*,³ who found that yttrium element congregated and remained at the interface to form a high $-Y_2O_3$ content of ZrO_2 , when ZrO_2 reacted with molten titanium.

After annealing at 1550°C for 6 h, the β' -Ti(Zr, O) in the reaction layer “V” became an ordered phase during cooling. The ordering of Zr and O in β' -Ti(Zr, O) caused the lattice strain owing to the difference in atomic size. As shown in the Fig. 5.6(b), the ordered β' -Ti(Zr, O) phase shows a high strain-field contrast because of the lattice distortion. Figure 5.6(c) and (d) show SADPs of β' -Ti(Zr, O) with the incident electron beam along the zone axes of $[021]$ and $[\bar{1}12]$, respectively. The ordered structure was characterized by the $\{\bar{1}1\bar{1}\}$ superlattice reflections of β' -Ti(Zr, O).

5.3.6 Variation in the reaction layer “VI”

Further into the ceramic side beyond the reaction layer “V,” the zirconia reacted with titanium to a less degree. The oxidation-reduction reaction rather than dissolution is the main mechanism in the reaction layer “VI.” It is believed that the dissolution played an insignificant role toward the formation of the reaction layer “VI” since the concentration of titanium was not detected in this layer.

Figure 5.7 shows the bright field images (BFI) of the reaction layer “VI” after annealing at 1100°, 1300°, 1400°, 1550°C for 6 h, respectively. After annealing at 1100°C/6 h, the limited reaction resulted in t - ZrO_{2-x} , as it was in as-hot pressed samples, with no intergranular α -Zr and insignificant grain

growth of zirconia [Fig. 5.7(a)]. At 1300°C/6 h, the t -ZrO_{2-x} still remained with a slight grain growth (grain size about 1~2 μm), while the dense α -Zr was formed by the exsolution of Zr from the metastable t -ZrO_{2-x} [Fig. 5.7(b)]. After annealing at 1400° or 1550°C, it was found that the lenticular t -ZrO_{2-x} with two variants precipitated in the c -ZrO_{2-x} matrix [Fig. 5.7(c) and (d)], which was stabilized by the extensive oxygen vacancies due to the interfacial reaction between Ti and ZrO₂. It was inferred that the specimen was cooled down from the two-phase ($c + t$) region in the ZrO₂-Y₂O₃ phase diagram.¹⁴ The lenticular t -ZrO_{2-x} precipitated in the c -ZrO_{2-x} matrix with three {100} variants as reported previously by Lin and Lin¹¹ in the Ti/ZrO₂ interface after annealing at 1550°C. The ordered c -ZrO_{2-x} also was identified by the 1/5{113} superlattice reflections. The grain sizes of zirconia after annealing at 1400° and 1550°C were about 8-10 μm and 20-30 μm, respectively, indicating rapid grain growth on annealing.

The microstructures of the reaction layer “VI” were different in the following respects: (1) the grain growth of zirconia; (2) the exsolution of α -Zr onto the grain boundaries of zirconia; (3) the morphologies and crystal structures of zirconia. Based upon the results shown in Fig. 5.1 and Fig. 5.7, the microstructural features of the reaction layer “VI” are summarized in Table 5.1.

5.3.7 Formation of suboxide Ti₃O above 1400°C

Some suboxides like Ti₃O would be formed due to the extended reaction between titanium and zirconia at high temperatures. Figure 5.8(a) shows the bright field image of Ti₃O, which contained stacking faults and dislocations, in α -Ti abutting the reaction layer “I” in the Ti/ZrO₂ interface after annealing at 1550°C for 6 h. No such a suboxide was found in those samples annealed at temperatures below 1400°C. The energy-dispersive

spectrum of Ti_3O in Fig. 5.8(b) revealed that it contained 75.21 at.% Ti, 1.38 at.% Zr, and 23.41 at.% O, being approximate to that of Ti_3O with Zr in solid solution. Figure 5.8(c) and (d) show the SADPs of the hexagonal Ti_3O with the electron beam parallel to the zone axes of $[2\bar{1}\bar{1}0]$ and $[1\bar{1}00]$, respectively. The superlattice reflections (0001) , $(\frac{1}{3}\frac{1}{3}\frac{2}{3}\frac{1}{2})$, and $(\frac{2}{3}\frac{2}{3}\frac{4}{3}\frac{1}{2})$ in Fig. 5.8(c) and (d) indicated the cell dimension along the c axis of the superlattice should be twice of the Ti cell, but not three times as proposed by Jostsons and Malin.¹⁵

The ordered structure of Ti_3O observed in this study coincided with the model proposed by Holmberg¹⁶ and Yamaguchi.¹⁷ It revealed that the structure of Ti_3O was a superstructure of the Ti_2O unit cell with the lattice parameters $a = \sqrt{3}a_o$ and $c = 2c_o$, where a_o and c_o were those of the host metal cell. Based on the crystal structure of Ti_2O , the oxygen vacancies in Ti_3O is in an ordered distribution that the oxygen position out of three in every oxygen layer normal to the c axis is vacant. The vacant positions have a zigzag arrangement in the direction of the c axis.

Figure 5.9 shows a unit cell of Ti_3O (dash line) and also that of the basic Ti_2O units (solid line). The Ti_3O structure data is described as follows:

Space-group: $P\bar{3}1c$ (No.163)

Unit cell dimensions: $a = 5.1411 \text{ \AA}$, $c = 9.5334 \text{ \AA}$

Unit cell content: 4 Ti_3O

2 O in $2(a)$: 0, 0, 1/4; 0, 0, 3/4

2 O in $2(d)$: 2/3, 1/3, 1/4; 1/3, 1/3, 1/4

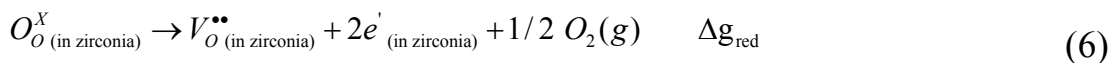
$$\begin{aligned}
& x, y, z; \bar{y}, x - y, z; y - x, \bar{x}, z; \\
& \bar{x}, \bar{y}, \bar{z}; y, y - x, \bar{z}; x - y, x, \bar{z} \\
12 \text{ Ti in } 12(i): & y, x, \frac{1}{2} + z; \bar{x}, y - x, \frac{1}{2} + z; x - y, \bar{y}, \frac{1}{2} + z \\
& \bar{y}, \bar{x}, \frac{1}{2} - z, x, x - y, \frac{1}{2} - z; y - x, y, \frac{1}{2} - z \\
& x = \frac{1}{3}; y = 0; z = 0.118
\end{aligned}$$

The oxygen has a large solubility in α -Ti at high temperatures from the Ti-O phase diagram.¹⁸ During cooling, the hexagonal phases of ordered titanium suboxides such as Ti₂O, Ti₃O, and possibly Ti₆O are formed within an extended range. In this study, only found was the ordered Ti₃O resulting from the transformation of α -Ti(O) during cooling.

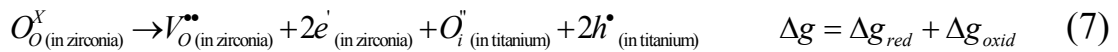
The thermodynamic consideration of the reaction between Ti and ZrO₂ is further discussed below. The following oxidation-reduction reactions between Ti and ZrO₂ are not thermodynamically favorable, because their Gibbs free energies are positive or slightly negative at 1727°C.¹⁹



However, these are not the cases in the present study. Based on the experimental results, the following reactions should be applied.¹¹



The resultant reaction is written by the summation of equations (5) and (6)



This reaction is thermodynamically favorable and the Gibbs free energy $\Delta g = \Delta g_{red} + \Delta g_{oxid} = -90.53(Kcal/mol)$ was calculated by Lin and Lin¹¹ at 1550°C. The fact the reaction (7) is thermodynamically favorable is consistent with the results observed in the present study. The ordered hexagonal phase Ti₃O was likely to be formed during the subsequent cooling of an extensive reaction between Ti and ZrO₂ at temperatures higher than 1400°C.

5.3.8 *Temperature effect on microstructural development*

The microstructure resulting from isothermal diffusion between titanium and zirconia is attempted to be explained by the help of the Ti-Zr-O ternary phase diagram. Assuming that the compositions of the solid phases are approximately constant between 1300° and 1550°C, the interpretation of the microstructure at the interface between Ti and ZrO₂ can be reasonably made in term of the isothermal Ti-Zr-O ternary phase diagram at 1450°C.²⁰ The Ti-Zr-O phase diagram and the diffusion couple are somewhat chemically different since the ZrO₂ contains 3 mol% Y₂O₃.²⁰ However, this probably does not have much effect on the results.

Figure 5.10 shows the microstructural evolution at the interface between titanium and zirconia diffusion couples annealed at 1300°, 1400°, and 1550°C, respectively, based upon the observation and analyses mentioned above. Figure 5.10(a) illustrates the titanium and zirconia diffusion couple prior to the anneal heat treatment, indicating the original interface and fine

ZrO₂ grains. When titanium is held in contact with zirconia at high temperatures, the reaction layers start to develop. Fig. 5.10(b) illustrates the diffusion paths, drawn in the Ti-Zr-O phase diagram,²⁰ of the Ti/ZrO₂ diffusion couple, isothermally annealed at 1300°, 1400°, and 1550°C, respectively. These diffusion paths connect all gross compositions at various cross sections along the longitudinal direction perpendicular to the interface. The dot, dash, and solid lines (marked as “1,” “2,” and “3,” respectively) are the diffusion paths of Ti/ZrO₂ on annealing at 1300°, 1400°, and 1550°C, respectively.

In Fig. 5.10(b), the diffusion path at 1300°C (dot line) crosses the fields of β -Ti, β -Ti + *t*-ZrO₂, α -Zr + β -Ti + *t*-ZrO₂, and α -Zr + *t*-ZrO₂. It is noted that the region of α -Zr + β -Ti + *t*-ZrO₂ in the Ti-Zr-O ternary phase diagram corresponds to the interface between the layers of β -Ti + *t*-ZrO₂ and α -Zr + *t*-ZrO₂. The reaction layers of β -Ti, β -Ti + *t*-ZrO₂, and α -Zr + *t*-ZrO₂ will be in sequence from Ti to ZrO₂ in the Ti-ZrO₂ diffusion couple on annealing at 1300°, as shown in the left schematic diagram of Fig. 5.10(c). During cooling, β -Ti(Zr, O) at the region away from the interface, dissolving a less amount of Zr, was transformed to α -Ti(Zr, O), where the continuous lamellar Ti₂ZrO was precipitated (designated as the reaction layer “I”). However, the β -Ti(Zr, O) at the region close to the interface, dissolving a larger amount of Zr, become a continuous β' -Ti(Zr, O) (designated as the reaction layer “IV”) during cooling. In the zirconia side, β' -Ti(Zr, O) and cubic ZrO_{2-x}, with highly concentrated yttrium (about 11.75 at% in this study), were formed in the reaction layer “V” during cooling. Further into the zirconia side, the α -Zr was precipitated along the grain boundaries of *t*-ZrO_{2-x}. Instead of *c*-ZrO_{2-x}, *t*-ZrO_{2-x} exists in the reaction layer “VI” because of the limited oxidation-reduction reaction at 1300°C, resulting in a less concentration of oxygen vacancies. The final microstructure on annealing and subsequent

cooling at 1300°C was schematically shown in the right of Fig. 5.10(c).

In contrast, the reaction layer “III” exists in the interface after annealing at 1400°C, but not at 1300°C. This is probably due to the fact that β -Ti dissolves more oxygen at 1400°C than at 1300°C. During cooling, the β -Ti(Zr, O) was transformed to β' -Ti(Zr, O), where the acicular α -Ti(Zr, O) was precipitated (designated as the reaction layer “III”). For comparison, t -ZrO_{2-x}, ordered c -ZrO_{2-x}, and intergranular α -Zr exist in the reaction layer “VI” because of an extensive oxidation-reduction reaction at 1400°C. The microstructure development on annealing and subsequent cooling at 1400°C was schematically shown in the right of Fig. 5.10(d).

The zirconia in the Ti-Zr-O ternary phase diagram, shown in Fig. 5.10(b), would be in the cubic phase instead of tetragonal phase when the Ti/ZrO₂ diffusion couple was isothermally annealed at temperatures above 1400°C as discussed above. Figure 5.10(b) reveals that the solid line or the diffusion path at 1550°C crosses the fields of β -Ti, α -Ti + β -Ti, β -Ti, β -Ti + c -ZrO₂, α -Zr + β -Ti + c -ZrO₂, and α -Zr + c -ZrO₂. The reaction layers of β -Ti, α -Ti + β -Ti, β -Ti, β -Ti + c -ZrO₂, and α -Zr + c -ZrO₂ would be observed in the Ti-ZrO₂ diffusion couple on annealing at 1550°C as shown in the left diagram of Fig. 5.10(e).

By comparing the diffusion paths for various temperatures, it is seen that the α -Ti(Zr, O) + β -Ti(Zr, O) two-phase region, where the diffusion path passes through, is found only at 1550°C. This region is corresponding to the reaction layer “II” in Fig. 5.1(d), consisting of β' -Ti and the lamellar Ti₂ZrO + α -Ti. During cooling, the β -Ti(Zr, O) was transformed to β' -Ti(Zr, O) and Ti₂ZrO was precipitated in α -Ti(Zr, O). In the zirconia side far away from the original metal-ceramic interface, ZrO₂ was dramatically reduced to

ZrO_{2-x} by titanium, accompanied by a significant grain growth of ZrO_{2-x} on heating. The intergranular α -Zr was excluded from the metastable oxygen deficient zirconia, while the lenticular *t*-ZrO₂ and ordered *c*-ZrO_{2-x} were formed from the *c*-ZrO_{2-x} matrix during cooling. The microstructures developed on annealing and subsequent cooling at 1550°C were schematically shown in Fig. 5.10(e).

According to the foregoing discussion, the reaction layers formed in the interface of titanium and zirconia at various temperatures were summarized in Table 5.2. It was seen that the oxidation and reduction reaction between Ti and ZrO₂ had a great tendency to form the α -Ti(O) and *t*-ZrO_{2-x}, even though only a limited interfacial reaction took place at temperatures as low as 1100°C. On the other hand, the formation of Ti₂ZrO, β' -Ti(Zr, O), Ti₃O, and the intergranular α -Zr as well as *c*-ZrO₂ were caused due to the extended reaction between Ti and ZrO₂ at higher temperatures such as 1400° and 1550°C. It is worth noting that the suboxide Ti₃O was sparsely found in the α -Ti(O), to the left of the reaction layer “I,” after annealing at temperatures above 1400°C. Also noted was an ordered β' -Ti(Zr, O) phase, along with disordered β' -Ti(Zr, O) + *c*-ZrO_{2-x}, existed in the reaction layer “V” in the interface after annealing at 1550°C/6 h. In addition, no cubic zirconia was found in the reaction layer “VI” after annealing at temperatures below 1300°C since a limited reaction gave rise to a lower concentration of oxygen vacancies and to a less degree of stabilization effect.

5.4 Conclusions

The diffusional reactions between titanium and zirconia were carried out isothermally in argon at temperatures between 1100° to 1550°C for 6 hours. The microstructure in the Ti/ZrO₂ interface depends strongly on the

temperature so that very distinct reaction layers are developed at various temperatures. A distinct three-phase layer, consisting of lamellar Ti_2ZrO + $\alpha\text{-Ti(O, Zr)}$ as well as $\beta'\text{-Ti(O, Zr)}$, was formed in the titanium side after annealing at $1550^\circ\text{C}/6$ h. Instead, a two-phase layer, consisting of the acicular $\alpha\text{-Ti(O)}$ and $\beta'\text{-Ti(Zr, O)}$, appeared after annealing at $1400^\circ\text{C}/6$ h. Neither the three-phase nor two-phase layer, was a $\beta'\text{-Ti(Zr, O)}$ founded in the Ti/ZrO_2 interface after annealing at $1300^\circ\text{C}/6$ h. In the zirconia side near the original interface, $\beta'\text{-Ti}$ coexisted with fine spherical $c\text{-ZrO}_{2-x}$, which dissolved a significant amount of Y_2O_3 in solid solution above 1300°C , due to the reaction enhanced dissolution mechanism. Further into the ceramic side, the zirconia grain grew significantly above 1400°C and the $\alpha\text{-Zr}$ was formed due to the exsolution of Zr out of the metastable ZrO_{2-x} after annealing above 1300°C . The $\alpha\text{-Zr}$ was densely distributed along with $t\text{-ZrO}_{2-x}$ at 1300°C , while it was continuously distributed at 1400°C and became coarsened at 1550°C both along grain boundaries of zirconia. The lenticular $t\text{-ZrO}_{2-x}$ was precipitated in the $c\text{-ZrO}_{2-x}$ matrix, which was stabilized by the extensive oxygen vacancies due to the interfacial reaction between Ti and ZrO_2 after annealing above 1400° , while the limited reaction resulted in $t\text{-ZrO}_{2-x}$ as it was in as-hot pressed samples at temperatures below 1300°C . Finally, the microstructural development in the Ti/ZrO_2 annealed at various temperatures was also described by the aid of the Ti-Zr-O ternary phase diagram.

Acknowledgment

The authors would like to thank the National Science Council of Taiwan for financially supporting this research under Contract No. NSC 93-2216-E-009-017. The authors would also like to pay their sincere appreciation to Mr. Chi-Ming Wen at Chung-Shan Institute of Science and Technology for preparing the hot-pressed specimens.

References:

1. G. Economos and W. D. Kingery, "Metal-Ceramic Interactions: II, Metal Oxide Interfacial Reactions at Elevated Temperatures," *J. Am. Ceram. Soc.*, **36**[12], 403-09 (1953).
2. B. C. Weber, W. M. Thompson, H. O. Bielstein, and M. A. Schwartz, "Ceramic Crucible for Melting Titanium," *J. Am. Ceram. Soc.*, **40**[11], 363-73 (1957).
3. R. Ruh, "Reaction of Zirconia and Titanium at Elevated Temperatures," *J. Am. Ceram. Soc.*, **46**[7], 301-06 (1963).
4. R. Ruh, N. M. Tallan, and H. A. Lipsitt, "Effect of Metal Additions on the Microstructure of Zirconia," *J. Am. Ceram. Soc.*, **47**[12], 632-35 (1964).
5. J. Zhu, A. Kamiya, T. Yamada, W. Shi, K. Naganuma, and K. Mukai, "Surface Tension, Wettability and Reactivity of Molten Titanium in Ti/Yttria-Stabilized Zirconia System," *Mater. Sci. Engng. A*, **A327**, 117-27 (2002).
6. B. C. Weber, H. J. Garrett, F. A. Mauer, and M. A. Schwartz, "Observations on the Stabilization of Zirconia," *J. Am. Ceram. Soc.*, **39**[6], 197-07 (1956).
7. C. L. Lin, D. Gan, and P. Shen, "Stabilization of Zirconia Sintered with Titanium," *J. Am. Ceram. Soc.*, **71**[8], 624-29 (1988).
8. K. F. Lin and C. C. Lin, "Transmission Electron Microscope Investigation of the Interface between Titanium and Zirconia," *J. Am. Ceram. Soc.*, **82**[11], 3179-185 (1999).
9. K. L. Lin and C. C. Lin, "Ti₂ZrO Phases Formed in the Titanium and Zirconia Interface after Reaction at 1550°C," *J. Am. Ceram. Soc.*, **88**[5], 1268-272 (2005).
10. K. L. Lin and C. C. Lin, "Microstructural Evolution and Formation Mechanism of the Interface between Zirconia and Titanium Annealed at

- 1550°C," accepted by *J. Am. Ceram. Soc.*, (2005).
11. K. L. Lin and C. C. Lin, "Zirconia-Related Phases in the Zirconia/Titanium Diffusion Couple after Annealing at 1100° to 1550°C," *J. Am. Ceram. Soc.*, **88** [10] 2928–934 (2005).
 12. G. Cliff and G. W. Lorimer, "The Quantitative Analysis of Thin Specimens," *J. Microsc.*, **130**[3], 203-07 (1975).
 13. R. F. Domagala, S. R. Lyon, and R. Ruh, "The Pseudobinary Ti-ZrO₂," *J. Am. Ceram. Soc.*, **56**[11], 584-87 (1973).
 14. H. G. Scoot, "Phase Relationships in the Zirconia-Yttria System," *J. Mater. Sci.*, **10**[9], 1527-35 (1975).
 15. A. Jostsons and A. S. Malin, "The Ordered Structure of Ti₃O," *Acta Cryst.*, **B24**[4], 211-13 (1968).
 16. B. Holmberg, "Disorder and Order in Solid Solution of Oxygen in α -Titanium," *Acta Chem. Scand.*, **16**, 1245-250 (1962).
 17. S. Yamaguchi, "Interstitial Order-Disorder Transformation in the Ti-O Solid Solution. I. Ordered Arrangement of Oxygen," *J. Phys. Soc. Japan*, **27**[1], 155-63 (1969).
 18. J. L. Murray and H. A. Wriedt, "The Oxygen-Titanium Phase Diagram"; pp. 2924-27 in *Binary Alloy Phase Diagrams Second Edition, Vol. 3*. Edited by T. B. Massalski, H. Okamoto, P. R. Subramanian, and L. Kacprzak. ASM International, Materials Park, OH, 1992.
 19. M. W. Chase, Jr., *NIST-JANAF Thermochemical Tables, 4th ed.*; National Institute of Standards and Technology, Gaithersburg, MA, 1998.
 20. M. Hoch, R. L. Dean, C. K. Hwu, and S. M. Wolosin, "Zirconium Plus Oxygen Plus Another Metal"; pp. 12 in *Phase Diagrams for Zirconium and Zirconia Systems*. Edited by H. M. Ondik and H. F. McMurdie. American Ceramic Society, Westerville, OH, 1998.

Table 5.1 Zirconia and intergranular α -Zr in the reaction layer “VI”

Annealing Conditions	Grain growth of zirconia and its size	Intergranular α -Zr	Morphology and crystal structure of zirconia
1100°C/6 h	Insignificant about 0.3~0.4 μm	Not found	equiaxed $t\text{-ZrO}_{2-x}$
1300°C/6 h	Insignificant about 1~2 μm	densely distributed	equiaxed $t\text{-ZrO}_{2-x}$
1400°C/6 h	Significant about 8~10 μm	grains delineated by α -Zr	$t\text{-ZrO}_{2-x}$ (lenticular) + $c\text{-ZrO}_{2-x}$ (ordered)
1550°C/6 h	Significant about 20 ~30 μm	Isolated and coarsened	$t\text{-ZrO}_{2-x}$ (lenticular) + $c\text{-ZrO}_{2-x}$ (ordered)

Table 5.2 Reaction layers formed in the interface of Ti/ZrO₂ at various temperatures

Phases	Layers	1100°C	1300°C	1400°C	1550°C
$\alpha\text{-Ti(O)}$		●	●	▲	▲
$\alpha\text{-Ti(Zr, O)} + \text{Ti}_2\text{ZrO}$	I	●	●	●	●
$\alpha\text{-Ti(Zr, O)} + \text{Ti}_2\text{ZrO} + \beta'\text{-Ti(Zr, O)}$	II	x	x	x	●
$\alpha\text{-Ti(Zr, O)} + \beta'\text{-Ti(Zr, O)}$	III	x	x	●	●
$\beta'\text{-Ti(Zr, O)}$	IV	x	●	●	●
$\beta'\text{-Ti(Zr, O)} + c\text{-ZrO}_{2-x}$	V	x	●	●	#
$\alpha\text{-Zr(O)} + t\text{-ZrO}_{2-x} + c\text{-ZrO}_{2-x}$	VI	x	†	●	●
$t\text{-ZrO}_{2-x}$		●	●	●	●

●: observed; x: none; ▲: with sparsely distributed Ti₃O; #: with ordered β' -Ti(Zr, O); †: no $c\text{-ZrO}_{2-x}$ was observed.

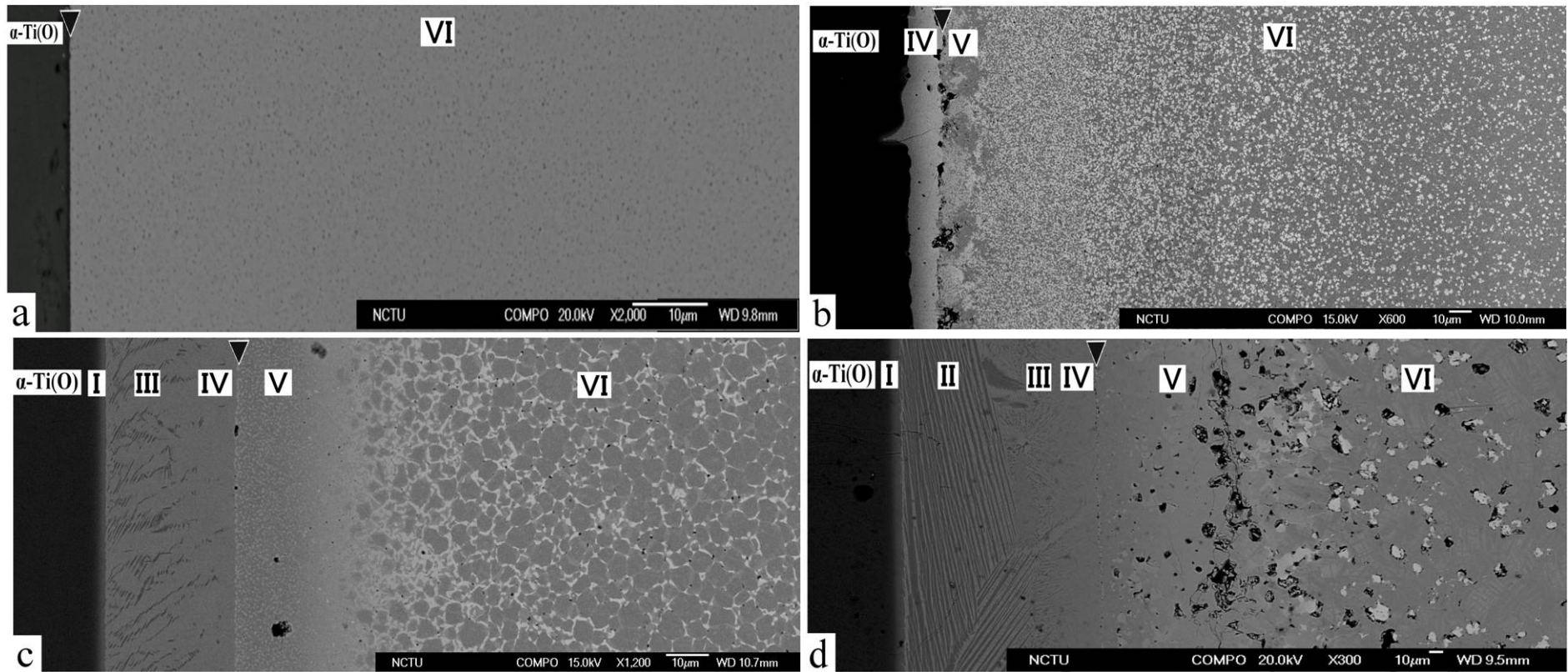


Fig. 5.1 SEM micrographs (backscattered electron image) showing the interface of Ti and ZrO₂ after reaction for 6 h at (a) 1100°; (b) 1300°; (c) 1400°; and (d) 1550°C. The vertical arrows in the upper side indicated the original interface. The interface reaction layers were designed as the layers “I”, “II”, “III”, “IV”, “V”, and “VI,” respectively.

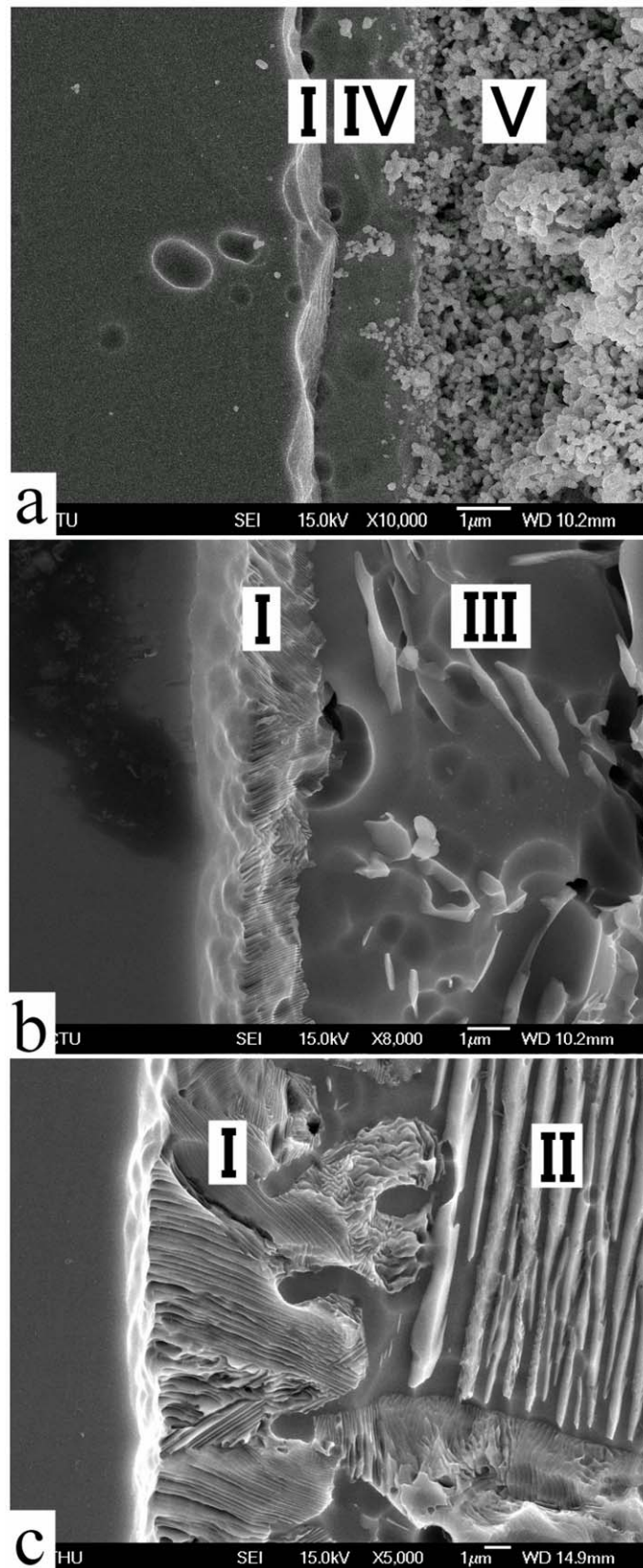


Fig. 5.2 SEM micrographs (secondary electron image) showing the variation of the layer “I” after reaction at (a) 1300°; (b) 1400°; and (c) 1550°C, respectively.

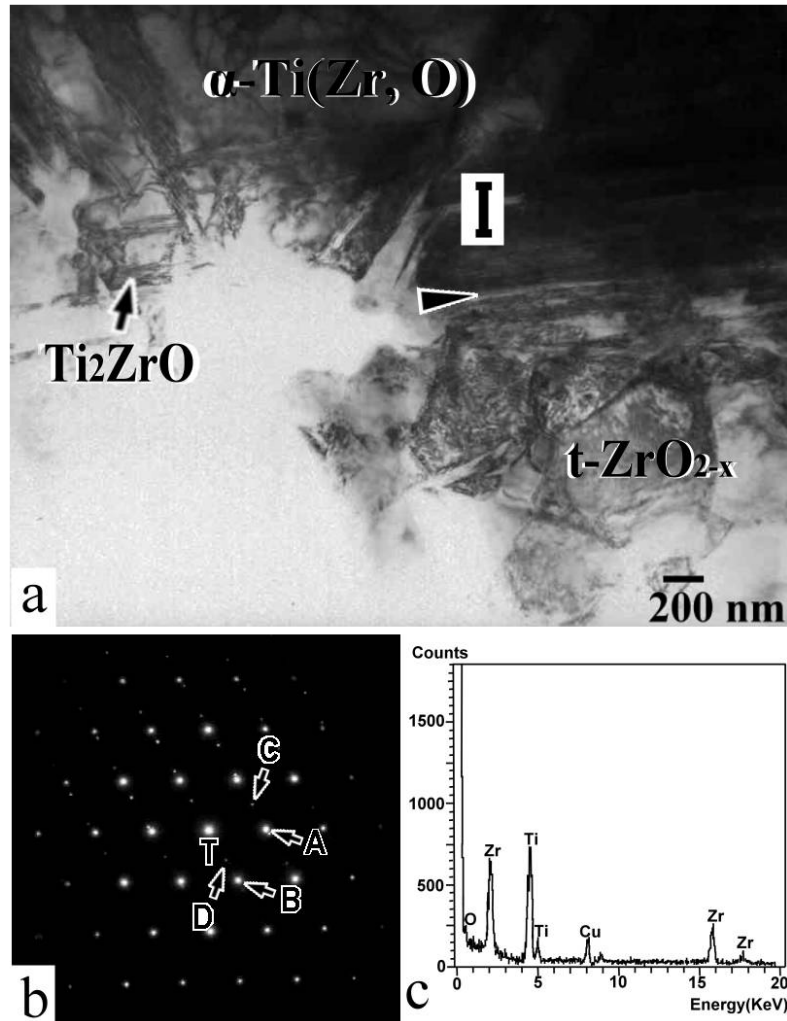


Fig. 5.3 (a) A TEM micrograph (bright field image, BFI) showing the layer “I” with the coexistence of $\alpha\text{-Ti}$ and Ti_2ZrO after reaction at $1100^\circ\text{C}/6\text{ h}$; (b) selected area diffraction patterns of the $\alpha\text{-Ti}$ and Ti_2ZrO , indicating that $[0001]_{\alpha\text{-Ti}} // [110]_{\text{Ti}_2\text{ZrO}}$ and $(10\bar{1}0)_{\alpha\text{-Ti}} // (1\bar{1}0)_{\text{Ti}_2\text{ZrO}}$ (A = $(01\bar{1}0)_{\alpha\text{-Ti}}$, B = $(10\bar{1}0)_{\alpha\text{-Ti}}$, C = $(00\bar{2})_{\text{Ti}_2\text{ZrO}}$, D = $(1\bar{1}0)_{\text{Ti}_2\text{ZrO}}$); (c) the energy-dispersive spectrum of Ti_2ZrO .

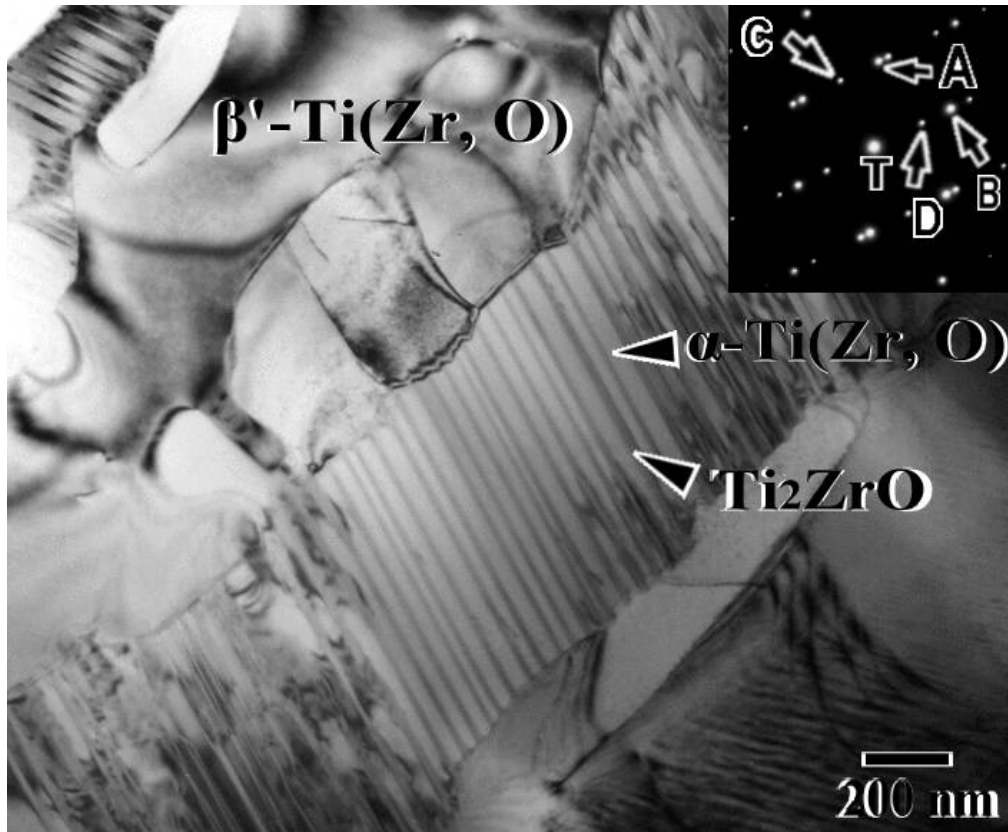


Fig. 5.4 TEM micrograph (bright field image, BFI) of the layer “II” showing the lamellae α -Ti + Ti_2ZrO and β' -Ti after reaction at 1550°C for 6 h; the inset selected area diffraction patterns indicate $[0001]_{\alpha\text{-Ti}} // [110]_{\text{Ti}_2\text{ZrO}}$ and $(10\bar{1}0)_{\alpha\text{-Ti}} // (1\bar{1}0)_{\text{Ti}_2\text{ZrO}}$ (A = $(01\bar{1}0)_{\alpha\text{-Ti}}$, B = $(10\bar{1}0)_{\alpha\text{-Ti}}$, C = $(00\bar{2})_{\text{Ti}_2\text{ZrO}}$, D = $(1\bar{1}0)_{\text{Ti}_2\text{ZrO}}$); (c) the energy-dispersive spectrum of Ti_2ZrO .

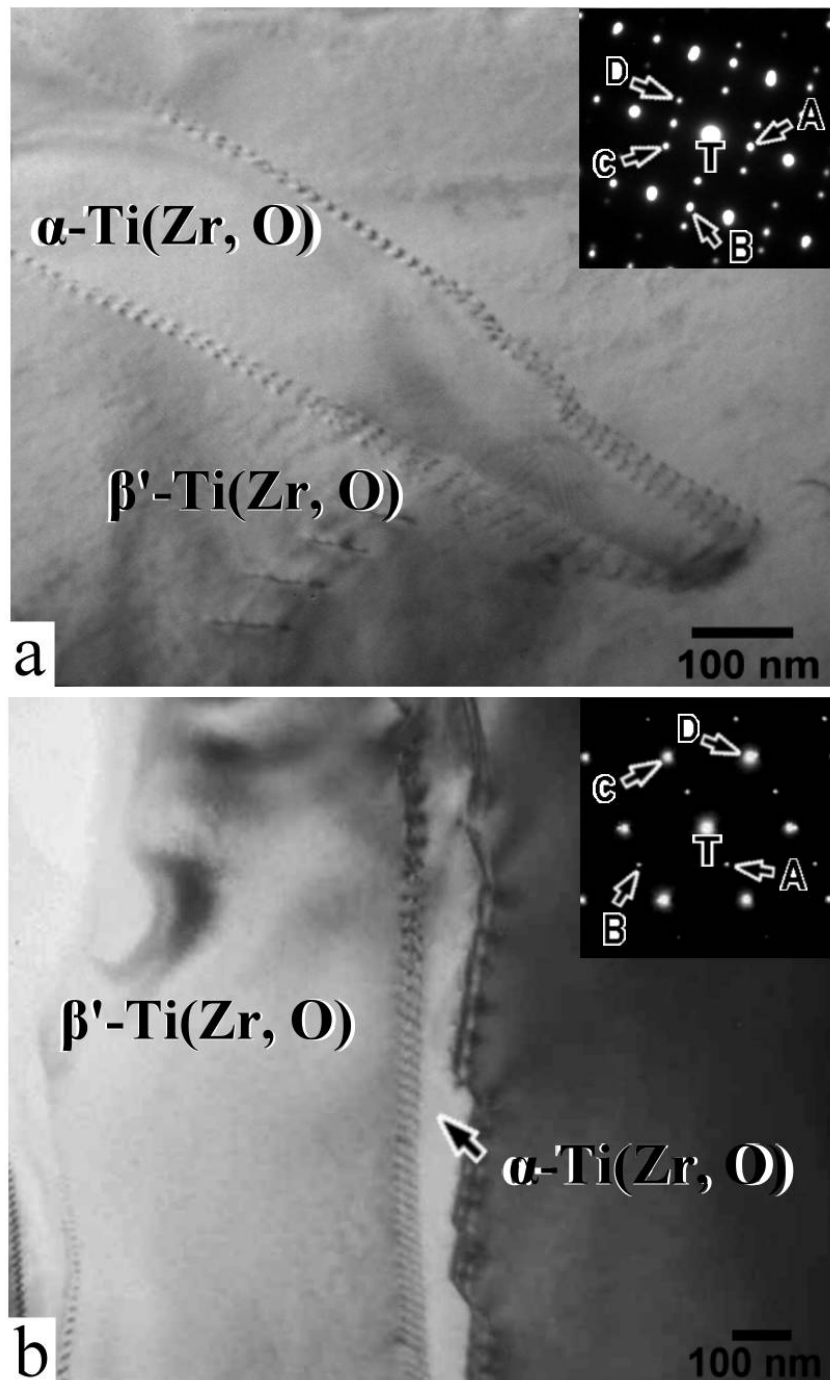


Fig. 5.5 TEM micrograph (bright field image, BFI) of the reaction layer “III” showing the coexistence of β' -Ti and α -Ti after reaction at (a) 1400°C/6 h (A = $(0001)_{\alpha\text{-Ti}}$, B = $(01\bar{1}0)_{\alpha\text{-Ti}}$, C = $(\bar{1}\bar{1}0)_{\beta'\text{-Ti}}$, and D = $(\bar{1}10)_{\beta'\text{-Ti}}$) in the inset selected area diffraction pattern (SADP) and (b) 1550°C/6 h (A = $(0001)_{\alpha\text{-Ti}}$, B = $(01\bar{1}0)_{\alpha\text{-Ti}}$, C = $(\bar{1}1\bar{2})_{\beta'\text{-Ti}}$, and D = $(11\bar{2})_{\beta'\text{-Ti}}$) in the inset SADP).

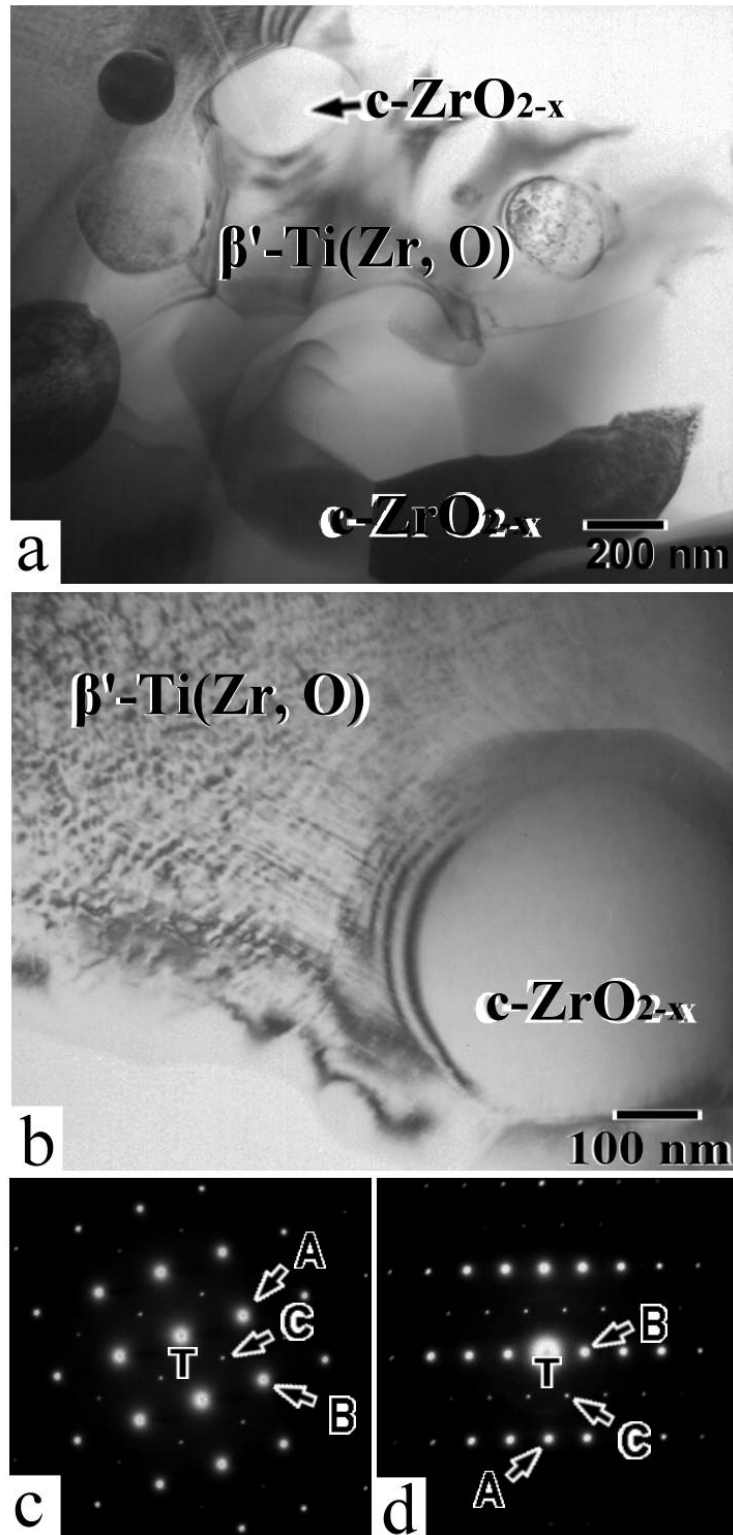


Fig. 5.6 TEM micrograph (bright field image, BFI) of the reaction layer "V" consisting of β' -Ti and c -ZrO_{2-x} after reaction at (a) 1400°C/6 h; (b) at 1550°C/6 h; (c) a selected area diffraction pattern (SADP) of β' -Ti in Fig. 5.6(b) (Zone axis is [021], A = $(\bar{2}00)$, B = $(\bar{2}2\bar{2})$, and C = $(\bar{1}1\bar{1})$); (d) a SADP of β' -Ti in Fig. 5.6(b) (Zone axis is $[\bar{1}12]$, A = $(\bar{1}3\bar{2})$, B = $(\bar{1}\bar{1}0)$, and C = $(\bar{1}1\bar{1})$).

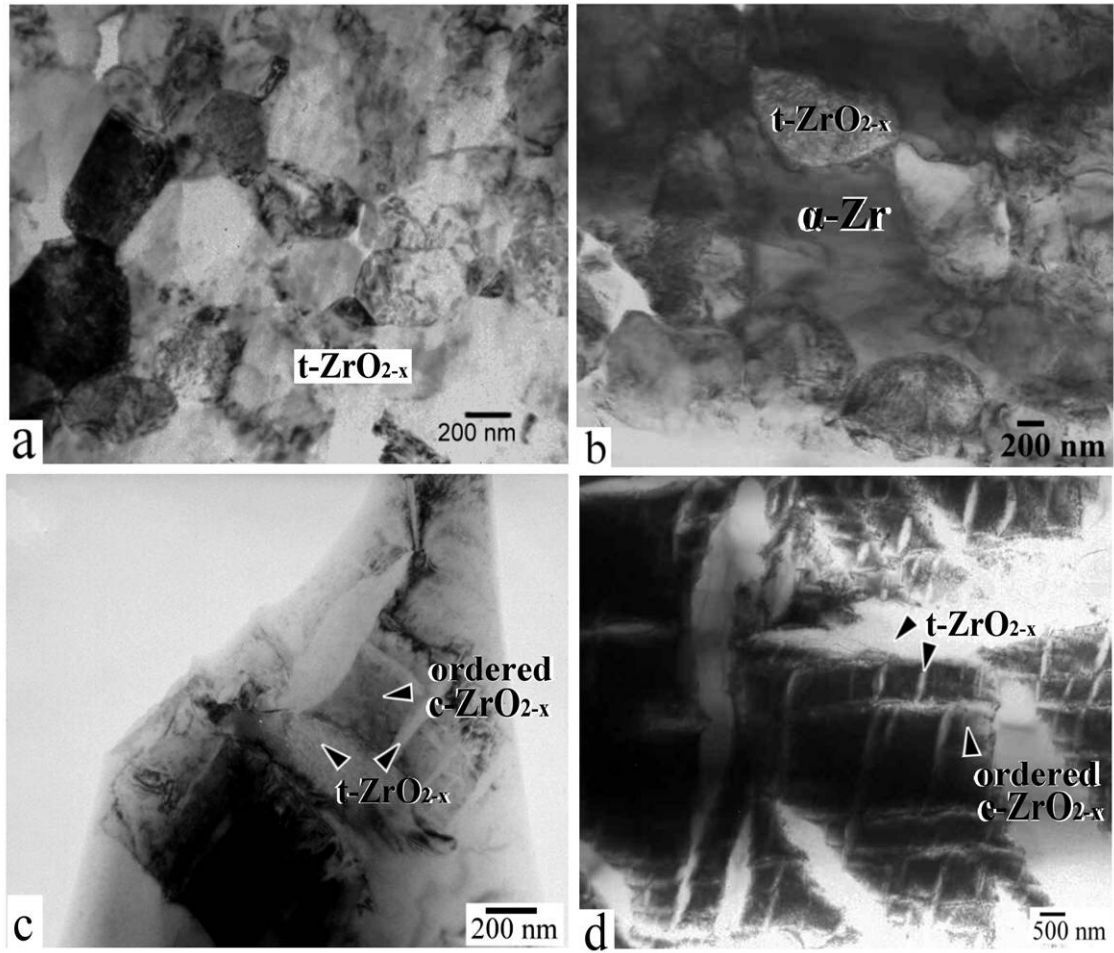


Fig. 5.7 TEM micrograph (bright field image; BFI) of the layer "VI" far away from the interface after reaction at (a) 1100°C, (b) 1300°C, (c) 1400°C, and (d) 1550°C for 6h.

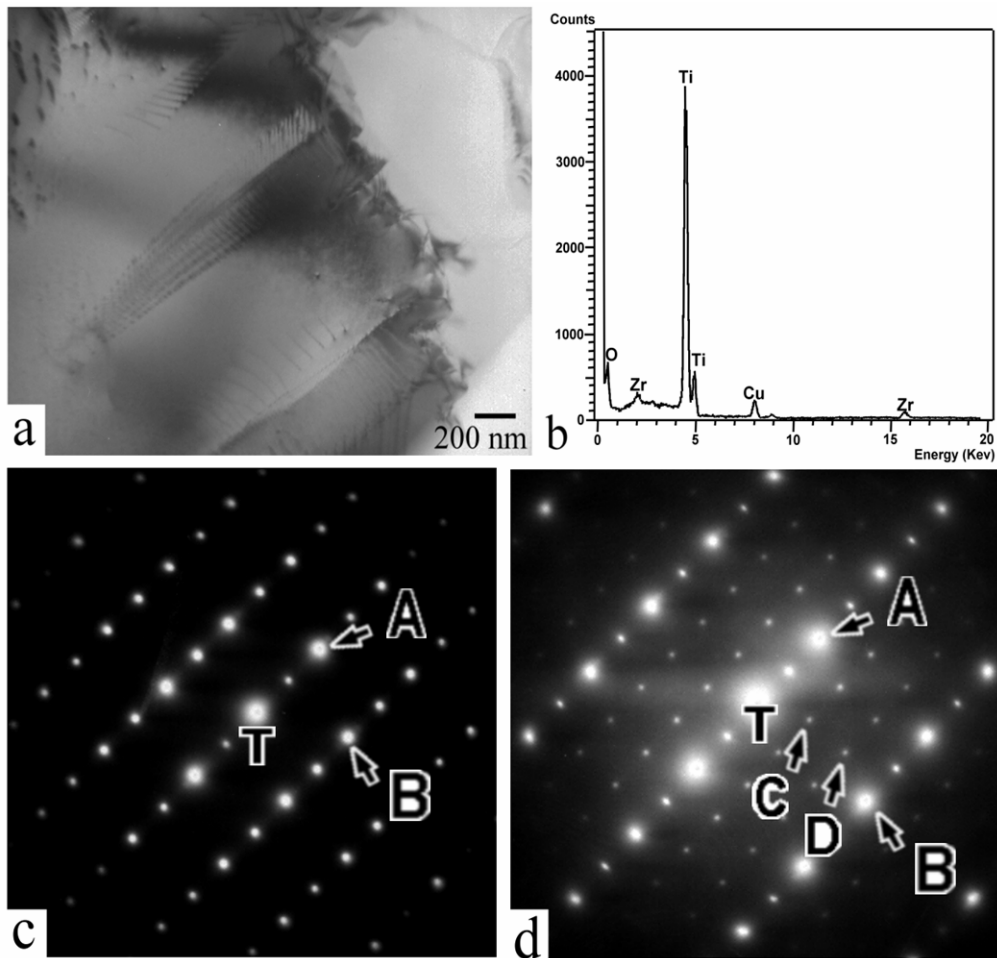


Fig. 5.8 (a) TEM micrograph (bright field image, BFI) of the suboxide Ti_3O near the reaction layer “I” after reaction at $1550^\circ C$ for 6 h; (b) the energy-dispersive spectrum of Ti_3O ; (c) the selected area diffraction pattern (SADP) along the $[2\bar{1}\bar{1}0]$ zone axis ($A = (0002)$ and $B = (0\bar{1}11)$); (d) a SADP of Ti_3O along the $[1\bar{1}00]$ zone axis. ($A = (0002)$, $B = (11\bar{2}0)$, $C = (\frac{1}{3}\frac{1}{3}\frac{2}{3}\frac{1}{2})$, and $D = (\frac{2}{3}\frac{2}{3}\frac{4}{3}\frac{1}{2})$).

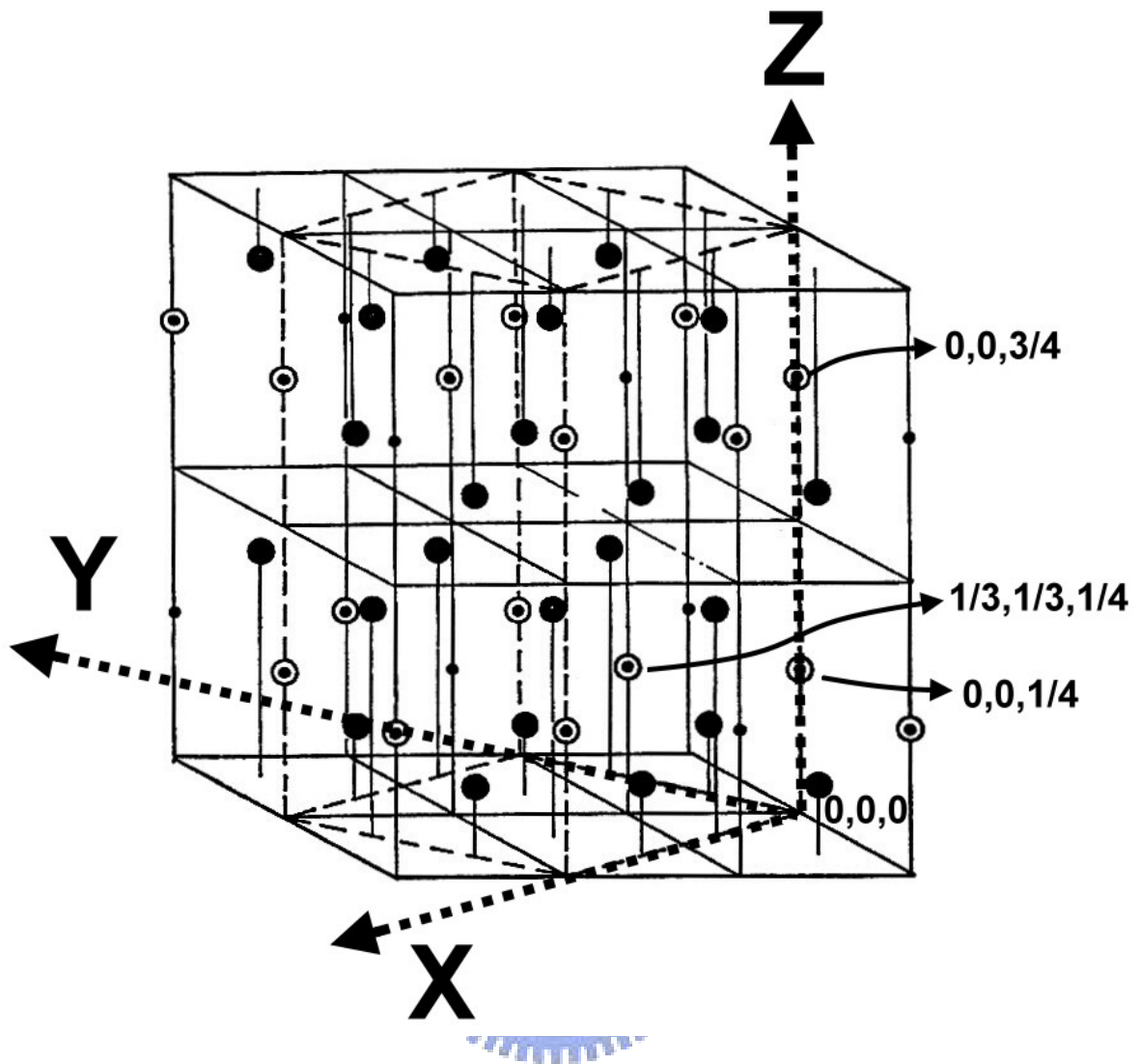
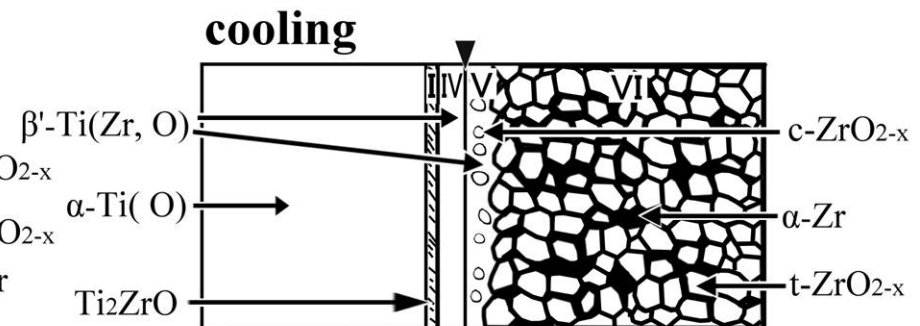
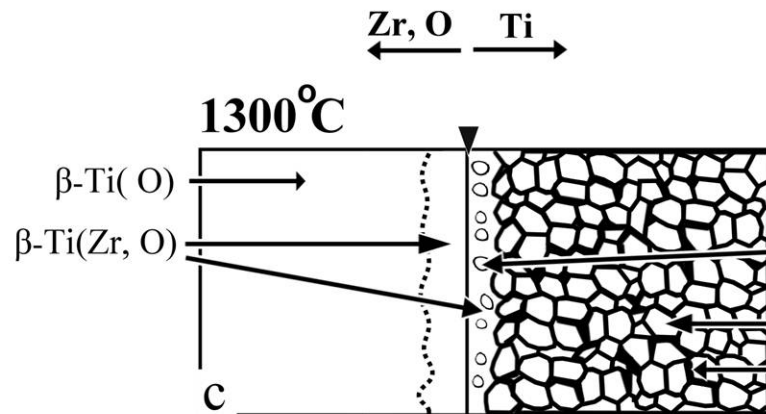
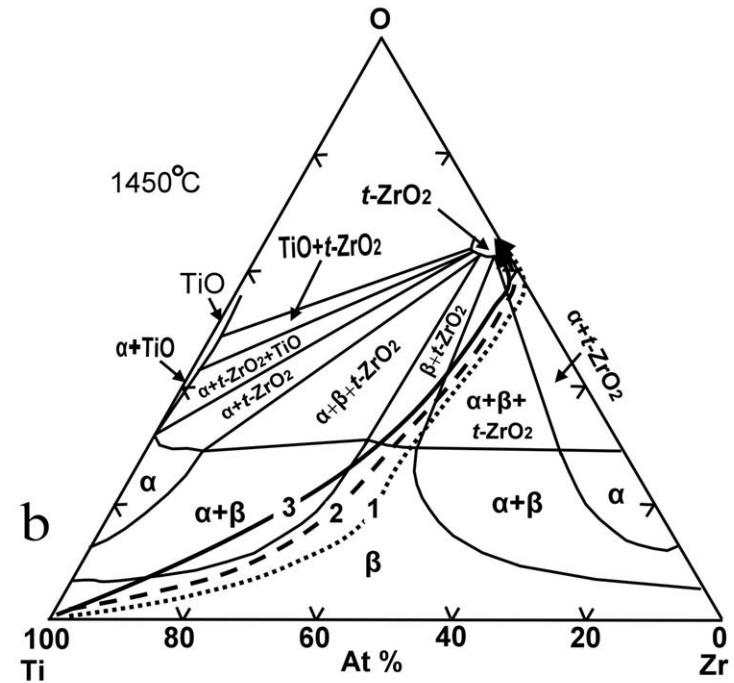
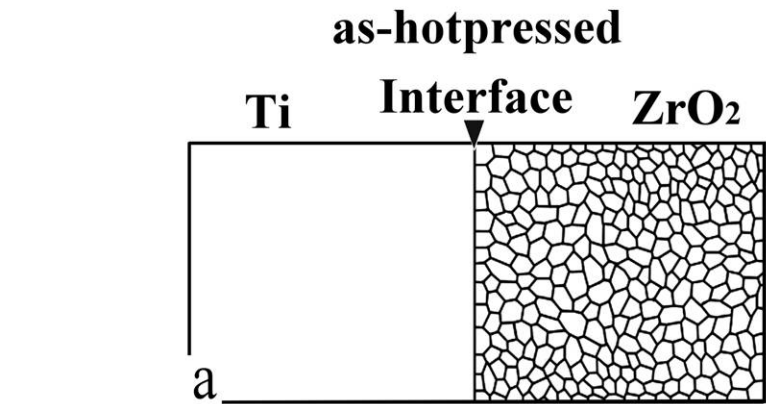


Fig. 5.9 The crystal structure of Ti_3O . The dash line indicates that the Ti_3O structure is based on the Ti_2O structure (solid line). \odot : oxygen position, \bullet : titanium position, \bullet : unoccupied oxygen position.¹⁵



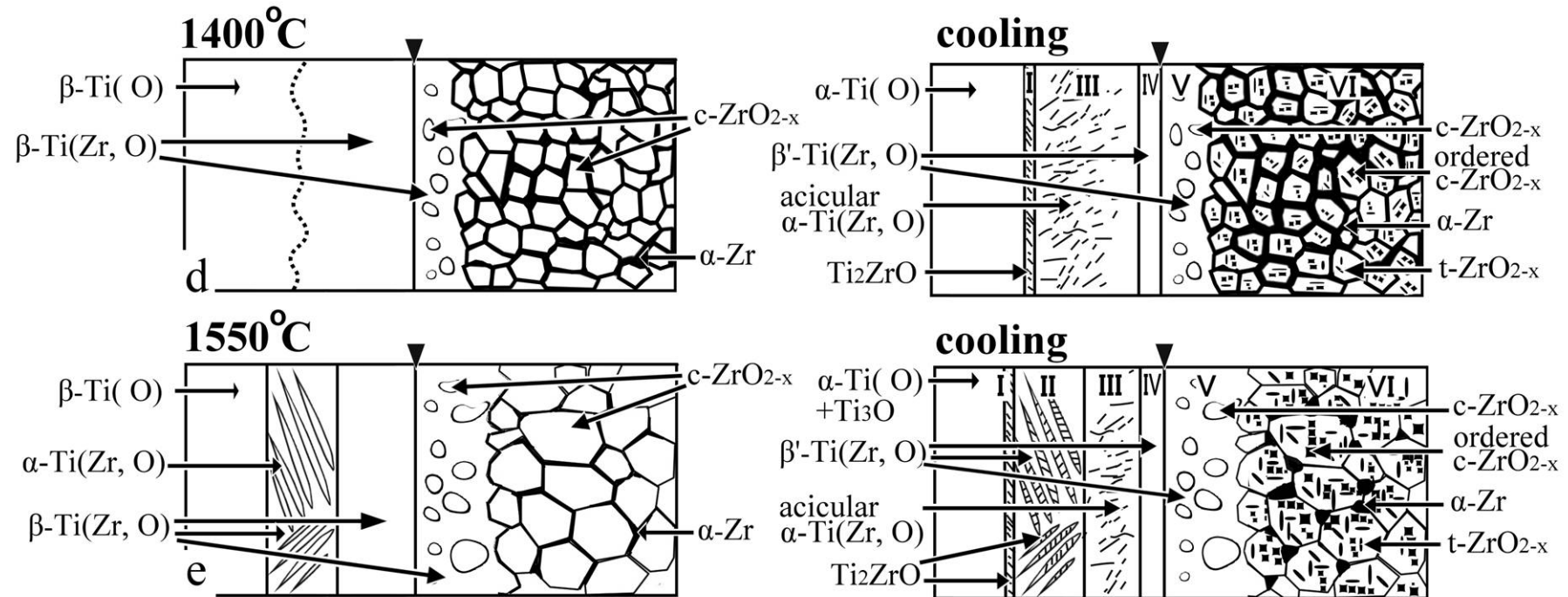


Fig. 5.10 Schematic diagrams showing the microstructural evolution of the Ti/ZrO₂ diffusion couple annealed at 1550°C. (a) as hot-pressed; (b) the relation between the Ti-Zr-O phase diagram.²⁰; (c), (d), and (e) the microstructure of Ti/ZrO₂ diffusion couple on annealing at 1300°, 1400°, and 1550°C and their cooling stages, respectively.